Alexandria Engineering Journal 106 (2024) 147–163

Contents lists available at ScienceDirect

Alexandria Engineering Journal

journal homepage: www.elsevier.com/locate/aej

Original article

Harnessing solar power: Innovations in nanofluid-cooled segmented thermoelectric generators for exergy, economic, environmental, and thermo-mechanical excellence

Hisham Alghamdi [a], Chika Maduabuchi [b,*], Kingsley Okoli [b], Mohana Alanazi [c], Hassan Fagehi [d], Mohammed Alghassab [e,*], Emad Makki [f,g,1], Mohammad Alkhedher [h]

[a] Electrical Engineering Department, College of Engineering, Najran University, Najran 55461, Saudi Arabia
[b] Artificial Intelligence Laboratory, Nsukka, Enugu 410001, Nigeria
[c] Department of Electrical Engineering, College of Engineering, Jouf University, Sakaka 72341, Saudi Arabia
[d] Department of Mechanical Engineering, College of Engineering, Jazan University, P.O. Box 706, Jazan 45142, Saudi Arabia
[e] Electrical Engineering Department, College of Engineering, Shaqra University, Riyadh 11911, Saudi Arabia
[f] Department of Mechanical Engineering, College of Engineering and Islamic Architecture, Umm Al-Qura University, Makkah 24382, Saudi Arabia
[g] Department of Ocean and Resources Engineering, School of Ocean and Earth Science and Technology, University of Hawaii at Manoa, Honolulu, HI 96822, United States
[h] Department of Mechanical and Industrial Engineering, Abu Dhabi University, Abu Dhabi 59911, United Arab Emirates

ARTICLE INFO

Keywords:
Thermoelectric generator
Nanofluid cooling
Solar energy conversion
Exergy efficiency
Structural integrity

ABSTRACT

Addressing the imperative need for advancements in thermoelectric generation, this study pioneers an analysis of nanofluid-cooled solar segmented thermoelectric generators with non-uniform cross-sections. Insights into thermal management, structural integrity, and economic efficiency in thermoelectric systems are provided, employing a numerical model that accurately represents thermoelectric effects by accounting for temperature dependencies of semiconductor materials. Through research, exploration of diverse coolant strategies, including TiO_2, Fe_3O_4, Al_2O_3, and graphene, offers key insights into their impact on cooling dynamics. Findings demonstrate that graphene nanofluid, operating at a flow velocity of 2 m/s, outperforms others, achieving optimal power generation of 221.77 mW and an exergy efficiency of 8.99 %. Additionally, at a concentrated irradiance of 595 kWm^{-2}, graphene leads in environmental benefits, with the highest CO_2 savings of 0.38 $kgyr^{-1}$, and demonstrates economic advantages with a cost-effective dollar per mW value of 3.79×10^{-6} $\$mW^{-1}$. Furthermore, the study verifies the structural integrity of these systems, with graphene achieving an optimal von Mises stress of 1.35 GPa at a semiconductor height of 0.2 mm. These advancements contribute to environmentally friendly and high-performance generators for sustainable energy solutions, paving the way for future innovations in thermoelectric technology.

1. Introduction

The renewable energy sector, crucial in addressing climate change and energy security, is rapidly evolving towards sustainable, carbon-neutral sources. This global shift, notable in countries like the United States, Nigeria, and Saudi Arabia, involves integrating renewable technologies into national energy strategies [1]. Thermoelectric Generators (TEGs), leveraging the Seebeck effect for direct heat-to-electricity conversion, are emerging due to their reliability, eco-friendliness, and silent operation. They are increasingly used in waste heat recovery, solar energy, and wearable sensors [2]. However, TEGs face challenges in efficiency and high costs of advanced thermoelectric materials [3], [4].

In TEG research, various strategies have been implemented to boost performance, including multi-staging [5], cascaded systems [6], phase change materials for thermal management [7], and semiconductor doping [8]. Notable techniques like non-uniform cross-section thermoelements [9] and material segmentation [10] show significant effectiveness. While recent efforts combining these strategies [11] have improved TEG efficiency in applications like waste heat recovery and

* Corresponding authors.
E-mail addresses: chika.maduabuchi.191341@unn.edu.ng (C. Maduabuchi), malghassab@su.edu.sa (M. Alghassab).
[1] *Orcid id:* http://orcid.org/0000-0002-2089-9776

https://doi.org/10.1016/j.aej.2024.06.064
Received 11 February 2024; Received in revised form 9 May 2024; Accepted 23 June 2024
Available online 9 July 2024

Nomenclature

Abbreviations

CEI	CO2 Emission Intensity
CI	Concentrated Solar Irradiance
CPC	Compound Parabolic Concentrator
DPW	Dollar Per Watt
FEM	Finite Element Method
IVC	Irregularly Variable Cross-Section
NCSSTEGs	Nanofluid-cooled solar segmented thermoelectric generators
NUCS	Non-uniform cross-sections
TEC	Thermoelectric Cooling
TEGs	Thermoelectric Generators
ZT	Figure-of-Merit

Symbols

[D]	Elasticity (stiffness) Matrix
A_f	Flow Area
Al_2O_3	Aluminium Oxide
α	Seebeck coefficient matrix (V/K)
$\vec{B}$	Coefficients of Thermal Expansion
β	Coefficient of Thermal Expansion
CO_2	Carbon di-oxide
C_p	Specific heat capacity (J/(kg·K))
C_n	Volumetric Cost
C_v	Heat Capacity at constant volume.
D	Electric flux vector (C/m^2)
$\vec{d}$	Displacement Vector
ΔT	Temperature Gradient
E	Young's Modulus
E^{el}	Electric field intensity vector (V/m)
Ex_{out}	Energy Output
Fe_3O_4	Iron Oxide
h	Heat Transfer Coefficient
J	Electric current density vector (A/m^2)
κ	Thermal conductivity matrix (W/(m·K))
Nu	Nusselt number
P_{TE}	Power output
Pr	Prandtl
P_y	Yearly Power
Q	Heat Energy
q	Heat flux vector (W/m^2)
Re	Reynolds
ρ	Density (kg/m^3)
$\vec{S}$	Stress Vector
S_{gen}	Entropy Generation
σ	Electrical conductivity matrix (S/m)
T	Absolute temperature (K)
TiO_2	Titanium Oxide
T_k	Temperature-related constant
u	Velocity
(B)	Wet Perimeter
ϕ	Electric scalar potential
$\vec{\varepsilon}$	Strain Vector
ϵ	Dielectric permittivity matrix (F/m).

concentrated solar energy conversion, research gaps remain. The following sections will detail these developments, highlight existing gaps, and outline the specific areas our paper addresses comprehensively.

Liu et al. [12] enhanced TEG design by using segmented thermoelements with asymmetric NUCS, achieving a 4.21 % increase in output power compared to uniform designs. Zhang et al. [13] further optimized TEGs with irregularly variable cross-section (IVC) thermoelements, resulting in a 51.71 % power enhancement over conventional segmented-IVC designs and a 7.57 % increase over unsegmented IVC systems. Luo et al. [14] explored the combined effects of geometry and contact resistance on segmented TEGs, highlighting the benefits of material segmentation with variable cross-sections. Shittu et al. [15] assessed thermo-mechanical performance in segmented TEGs under pulsed heat flux, reducing von Mises stress by 7.45 % and 39.21 % on the hot and cold sides, respectively, compared to unoptimized systems.

TEG performance is influenced by various factors, including semiconductor material properties, thermoelement geometry, and crucially, the temperature gradient across its hot and cold junctions. Effective cooling, traditionally achieved using air [16], is vital for temperature regulation and heat sinking. Recent studies have focused on water and nanofluids as superior alternatives for cooling. Notable research includes Wiriyasart et al.'s [17] exploration of titanium oxide nanofluids and ferrofluids in thermoelectric cooling, reducing temperature differentials by up to 9.6 %. Li et al. [18] observed power output improvements in automotive exhaust TEG systems using Ethylene glycol-based nanofluids. Hilmin et al. [19] found that titanium oxide nanofluids boosted efficiency and power in automotive exhaust TEG systems. Finally, Xing et al. [20] demonstrated a significant increase of 26.93 % in power and 14.74 % in efficiency using graphene nanofluid cooling at 0.1-wt% concentration.

Building upon the advancements in cooling technologies observed in recent studies, the integration of photovoltaic-thermoelectric (PV-TE) systems with graphene nanofluid cooling presents a promising avenue for enhancing both power output and efficiency.

In a comprehensive review of literature focusing on nanofluid utilization as a cooling medium [21], the potential of nanofluids for enhancing the performance of photovoltaic-thermal (PV/T) systems as observed by Aberoumand et al. [22] displays the capacity of nanofluids to augment both energy and exergy efficiencies within such systems. In their investigation, Alghamdi et al. [23] observed a notable 12 % increase in electric power output by employing a multi-stage segmented rectangular configuration in a photovoltaic-thermoelectric generator system, demonstrating enhanced thermal management particularly at a flow velocity of 2 m/s, illustrating the superior performance of graphene nanofluid. In their investigation into nanofluid cooling augmentation, Ruan et al. [24] demonstrated notable enhancements in output power and conversion efficiency of a thermoelectric generator system. Through the substitution of water cooling with a 0.1 wt% nanofluid at$Re = 100$, they observed an increase of 11.38 % in output power and 5.7 % in conversion efficiency. The integration of graphene nanofluid cooling with photovoltaic-thermoelectric systems represents a promising approach for augmenting power output and efficiency, leveraging recent advancements in cooling technologies. Furthermore, the current research aims to build upon these findings by providing a comprehensive analysis of the performance and optimization of nanofluid-cooled thermoelectric generators, offering further insights into the potential of nanofluid-based cooling strategies in enhancing the efficiency and sustainability.

Our study aims to fill voids in the existing knowledge base through thorough and detailed investigations. With the goal of shedding light on unresolved areas within the discipline, this research endeavors to rectify some deficiencies through:

1. Holistic Analysis: Our study aims to fill a critical gap in existing research by conducting a comprehensive analysis of nanofluid-

cooled thermoelectric generator systems. While previous studies have focused primarily on traditional bismuth-telluride modules, our research extends to explore the potential of advanced segmented modules with nanofluid cooling. By examining the exergy, economic, and thermo-mechanical aspects of these systems, we provide a more complete understanding of their performance dynamics.

2. Exploration of Novel Parameters: We seek to advance the current understanding of TEG systems by exploring novel parameters, such as semiconductor cross-sections and nanofluid coolant strategies. Through our investigation of various nanofluids, including TiO_2, Fe_3O_4, Al_2O_3, and graphene, we aim to shed light on their impact on cooling dynamics and overall system performance. By considering these factors, we aim to push the boundaries of TEG design and optimization.
3. Contribution to Sustainable Energy Solutions: Our research contributes to the advancement of sustainable energy solutions by offering insights into the viability of innovative TEG designs. By addressing gaps in exergy and economic assessments, environmental impact quantification, thermo-mechanical assessments, comprehensive device design exploration, and realistic thermal management considerations, we pave the way for more efficient and environmentally friendly TEG systems.

By recognizing gaps in the existing body of knowledge and conducting a meticulous investigation, this study endeavors to offer invaluable insights, thus advancing the frontier of research in the field. The significance of this research is shown by the need to comprehensively understand the performance of nanofluid-cooled solar segmented thermoelectric generators with non-uniform cross-sections, an area that has been relatively underexplored in the literature. With a focus on exergy, economic, environmental, and thermo-mechanical dimensions, our study aims to fill this critical void and drive progress in thermoelectric technology towards more sustainable energy solutions.

Beginning with an in-depth look at thermoelectric materials and computational models in 'Materials and Methods,' we establish the groundwork for our study. The 'Theoretical Framework' section lays out the mathematical equations guiding our finite element method optimization. We then present our 'Results and Discussion,' where we analyze and validate our findings against previously published data. Concluding with key takeaways and future research directions, we aim to enhance understanding and inspire further advancements in this evolving field.

2. Materials and methods

In this section, details of the methodology, materials, and configurations for the segmented TEG model are provided emphasizing transparency and replicability. Using advanced modeling, the study explores innovative TEG performance strategies, offering insights for future research in thermoelectric technology.

2.1. System description

This study investigates the dynamics of a nanofluid-cooled solar segmented thermoelectric generators (NCSSTEGs) with non-uniform cross-sections (NUCS), as shown in Fig. 1. The figure features a thermocouple element for accurate computational results since the system is electrically connected in series and thermally in parallel. A compound parabolic concentrator (CPC) with varying solar concentration ratios is utilized to magnify the amount of solar irradiance incident on the device hot junction [25]. Global solar irradiance, modelled according to AM 1.5 G weather conditions, is focused onto the TEG's top ceramic plate. This flux is converted into thermal energy at the hot junction using a selective surface absorber, matched in area with the top ceramic plate to ensure uniform temperature distribution. The ceramic plates, made of 96 % alumina, are chosen for their superior thermal properties. The thermoelectric legs of the study consist of bismuth-telluride (BiTe) for the cold segment and skutterudite (SKT) for the hot segment. Skutterudite exhibits optimal performance under high temperatures, up to 1000 K. Detailed material property data are available in references [26, 28] and plotted in Fig. 2 for further comprehension. Copper conductor pads in the study are used to direct electrical energy from the thermoelectric legs to the external load, optimized for maximum power by matching the load to the internal resistance of the thermoelectric material. Lead-free solder interconnectors join the legs to the conductor pads, providing sturdy connections. The properties of these materials are summarized in Tables 1 and 2. To enhance the TEG system performance, various nanofluids with unique thermophysical properties were tested as coolants. These included Distilled Water, TiO_2, Fe_3O_4, Al_2O_3, and Graphene, selected for their potential to improve system efficiency. The key properties of these nanofluids - thermal conductivity, kinematic viscosity, density, and specific heat - were sourced from literature and are detailed in Table 3. The thermophysical properties of the selected nanofluids are crucial in defining convective boundary conditions and

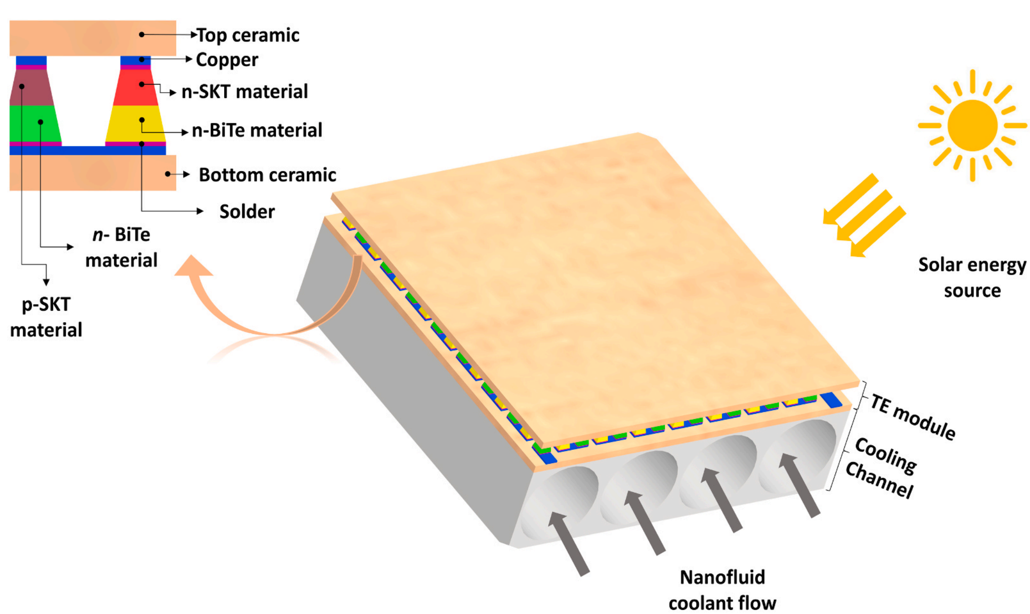

Fig. 1. Conceptual model of the thermoelectric module.

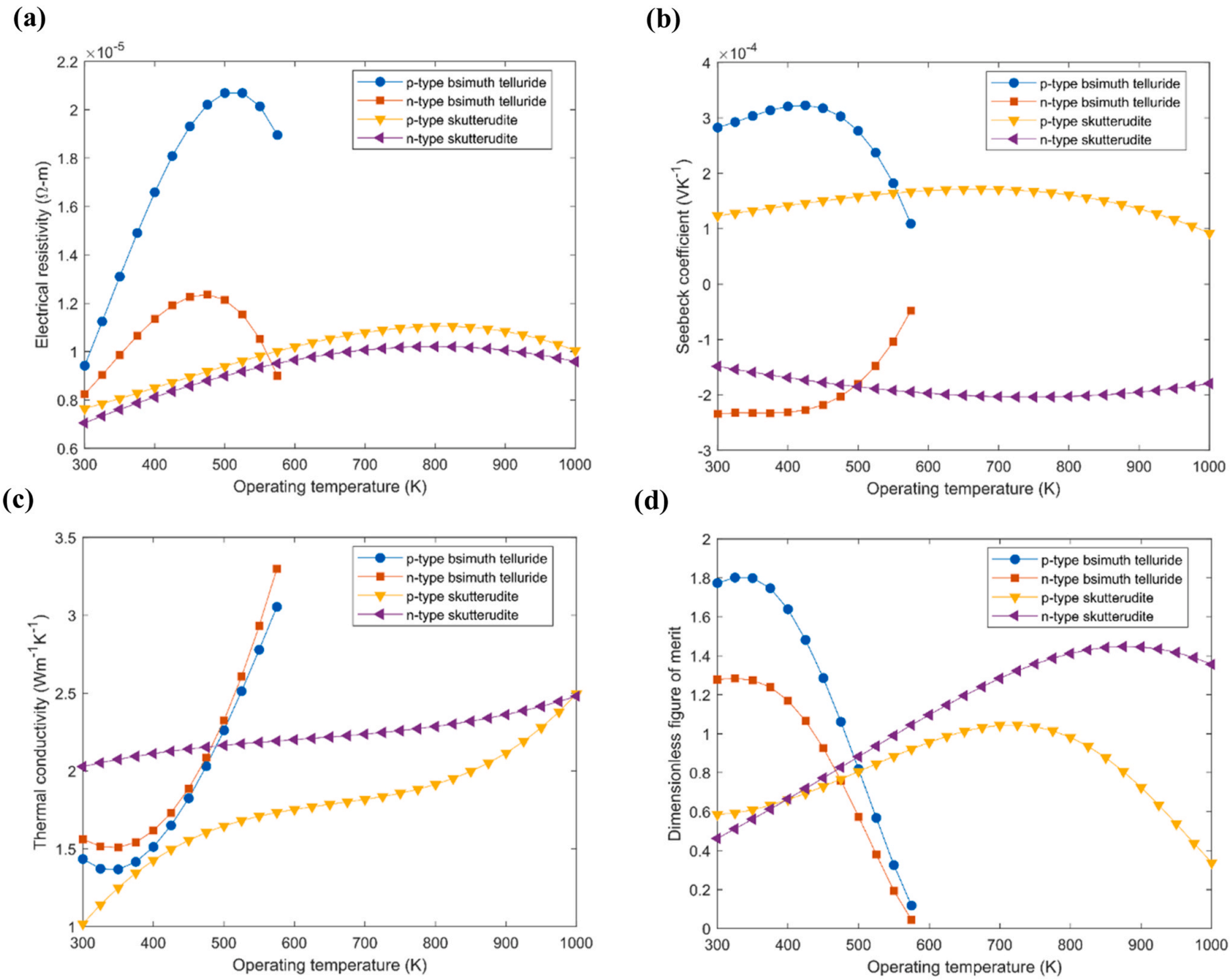

Fig. 2. Behaviour of the thermoelectric material properties as the operating temperature in the segments change [26], [27], [28] (a) electrical resistivity (b) Seebeck coefficient (c) thermal conductivity (d) dimensionless figure of merit.

Table 1
Identified Research Gaps in TEG Performance Optimization.

Gap Number	Research Gap	Description
1	Exergy and Economic Analysis	Lack of holistic exergy and economic assessments for commercial viability and effectiveness.
2	Environmental Impact	Absence of quantification on CO_2 emission savings, crucial in the context of sustainable solutions.
3	Thermo-mechanical Assessment	Limited scope in existing studies, not fully addressing transient environmental conditions.
4	Comprehensive Device Design	Focus predominantly on asymmetrically coupled segments, missing broader design evaluations.
5	Realistic Thermal Management	Over-simplification with constant cold junction temperature assumptions, not reflecting practical operating conditions.

evaluating cooling behavior on the TEG's cold side, directly impacting system performance. The upcoming sections analyze these aspects, employing these properties and empirical correlations to model the TEG's cooling performance effectively.

2.2. Theoretical framework

The governing equations of thermoelectricity are presented in this section alongside the expressions used to determine the performance of the proposed device.

2.2.1. Governing equations of thermoelectricity

Thermoelectric analysis studies the coupled behavior of heat flow and electric charge continuity. The equations governing these phenomena can be expressed as [28], [39], [40],:

Heat Flow Equation:

$$\dot{q} = \rho C_p \frac{\partial T}{\partial t} + \nabla . q \tag{1}$$

Continuity of Electric Charge:

$$0 = \nabla . \left(J + \frac{\partial D}{\partial t} \right) \tag{2}$$

Thermoelectric Constitutive Equations [41], [42]:

Heat flux related to electric current:

$$q = \Pi . J - \kappa . \nabla T \tag{3}$$

Electric current related to electric and temperature field

$$J = \sigma \cdot (\nabla \phi - \alpha \cdot \nabla T) \tag{4}$$

Table 2
Thermal and Physical Properties of the Materials [29], [30], [31], [32], [33], [34], [35].

Materials	κ (W/m·K)	σ (S/m)	C_p (J/kg·K)	ρ (kg/m^3)	β (1/K)	E (GPa)	p	S (V/K)
Ceramic	25	1×10^{-12}	800	3970	0.68×10^{-5}	340	0.22	-
Copper	385	5.9×10^{7}	386	8930	1.7×10^{-5}	120	0.3	6.5×10^{-6}
Solder	55	2×10^{7}	210	7240	2.7×10^{-5}	44.5	0.33	-
Bi_2Te_3	–	–	154.4	7740	0.8×10^{-5}	65–59	0.23	$f(T)$
$CoSb_3$	–	–	238.7	7582	6.36×10^{-6}	145.38	0.223	$f(T)$

Table 3
Thermophysical Properties of Coolant Fluids [36], [37], [38].

Fluids	κ (W·m^{-1}·K^{-1})	ν (10^{-7}m^2·s^{-1})	ρ (kg·m^{-3})	C_p (J·kg^{-1}·K^{-1})
Distilled Water	0.6	7.47797	997	4181.7
TiO_2	0.607	9.2143	1048	3502
Fe_3O_4	0.6274	8.174939	1003.06	4178.485
Al_2O_3	0.661	10.07544	1007.4	4154.7
Graphene	0.752	9.97062	1123.3	3343.188

Electric flux related to the electric field in dielectric medium

$$D = \epsilon \cdot E^{el} \tag{5}$$

Electric field is irrotational and related to the electric scalar potential

$$E^{el} = -\nabla\phi \tag{6}$$

Eqs. (1)-(6) are then further combined and manipulated to form a system of coupled equations of thermoelectricity:

Coupled Equations of Thermoelectricity [43], [44]:

Heat flow with heat generation term:

$$\dot{q} = \rho C_p \frac{\partial T}{\partial t} + \nabla.(\Pi.J - \kappa.\nabla T) \tag{7}$$

Electric charge continuity with displacement current [45], [46]:

$$0 = \nabla.\left(\sigma\cdot(\nabla\phi - \alpha\cdot\nabla T) + \frac{\partial(\epsilon\cdot E^{el}\ \ )}{\partial t}\right) \tag{8}$$

The heat generation term in Eq. (8) includes the electric power spent on Joule heating and on work against the Seebeck field.

2.2.2. Energy (Power), Exergy, Economic, and Environmental Assessments

This methodology outlines a multi-dimensional approach to assess thermoelectric generator systems, encompassing power output, exergy efficiency, environmental impact, and economic feasibility. It provides a theoretical basis for investors, scientists, and policymakers in designing and evaluating TEG systems, aligning technological advancements with environmental and socio-economic objectives for sustainable and viable thermoelectric generation.

The electrical power output of a thermoelectric generator can be modelled as a function of the Seebeck coefficient, S, the temperature difference across the TEG (ΔT), and the internal resistance, R, under maximum power transfer theorem is calculated as follows [47]:

$$P_{TE} = \frac{(S\Delta T)^2}{4R} \tag{9}$$

Exergy analysis is pivotal in evaluating thermodynamic efficiency. Exergy analysis deals with the quality of energy within the system, considering entropy and energy degradation. An exergy balance must be carried out to account for all the exergy flows and destruction within the system, including chemical exergy, physical exergy, and more. The exergy balance is defined as [48]:

$$Ex_{in} = Ex_{out} + Ex_{loss} \tag{10}$$

where Ex_{in} is the exergy input, Ex_{out} is the exergy output, and Ex_{loss} is the exergy lost due to irreversibility. These exergy terms are defined as follows [49]:

$$Ex_{in} = CIA\tau\left[1 - \frac{4}{3}\left(\frac{T_a}{T_s}\right) + \frac{1}{3}\left(\frac{T_a}{T_s}\right)^4\right] \tag{11}$$

where CI is the concentrated solar irradiance (assuming AM 1.5 G conditions), A is the surface area of the top alumina plate, and τ is the efficiency of the optical concentrating system. T_a is the temperature of the surroundings (295.15 K) and T_s is the Sun's black body temperature (5778 K).

The exergy lost due to irreversibility is evaluated through the entropy generation, S_{gen}, as follows [50]:

$$Ex_{loss} = T_a S_{gen} \tag{12}$$

Ex_{out} typically represents the rate of energy output, or the energy flow leaving a system per unit of time. In the context of a TEG system, this could be defined as the electrical power output (P_{TE}).

Therefore, the exergy efficiency is the measure of how effectively the system converts available exergy into desired output. Here, exergy efficiency is described as [51]:

$$\eta_{ex}\frac{P_{TE}}{Ex_{in}} \tag{13}$$

An examination of the environmental footprint can be assessed by calculating the CO_2 emissions [52]:

$$CO_2 P_y \times CEI \tag{14}$$

where CEI is the CO_2 emission intensity (0.475 $kgCO_2eq/kWh$ [53]), and P_y is the yearly power generation, considering 365 days of operation and an average sunshine hour of 8 h. This equation builds on the sustainability goals of thermoelectric technology.

The economic feasibility can be determined by evaluating the dollar per watt (DPW) generated [54]:

$$DPW = \frac{1}{P_{TE}} \times \sum_{n=1}^{N} C_n V_n \qquad 15)$$

where V_n and C_n are the volume and volumetric cost of N total thermoelectric elements, respectively. This equation integrates supply chain management and cost optimization into thermoelectric generator design.

2.2.3. Finite element formulation

The finite element method (FEM) provides a numerical solution to these coupled equations by discretizing the domain into elements and approximating the solution within each element.

2.2.4. Approximations

The temperature T and electric scalar potential ϕ are approximated over a finite element as [55]:

$$T = N\cdot T_e \tag{9}$$

$$\phi = N\cdot\phi_e \tag{10}$$

where N are shape functions, and T_e and ϕ_e are nodal temperature and electric potential vectors, respectively.

a) Weak Projective Form:
The system of equations is then written in a weak projective form, integrated by parts, and combined with boundary conditions to obtain the thermoelectric finite element equations.
b) Element Matrices and Load Vectors:
The element matrices and load vectors are calculated by numerical integration (using Gauss quadratures) over the element volume. These include stiffness matrices, damping matrices, and load vectors representing thermal loads, electric power, Peltier loads, etc.
c) Global Matrix Equation:
The global matrix equation is assembled from individual finite element equations. Since the thermal load depends on the electric solution, the analysis is nonlinear, and iterations are required to converge.
d) Solution:
The solution yields temperatures and electric potentials at nodes. From these, gradients such as the temperature gradient and electric field are calculated, allowing the determination of fields like J, q, D, and Joule heat generation density.
e) Deformation and Stress Distribution:

To evaluate deformation and stress due to thermal expansion, the same coupled-field elements can be used to perform a structural-thermal-electric analysis.

Finite Elements Used [56]:

- **PLANE223**: 2-D 8-node quadrilateral
- **SOLID226**: 3-D 20-node hexahedron
- **SOLID227**: 3-D 10-node tetrahedron

These elements allow for various modeling capabilities including 2-D plane behavior, 3-D axisymmetric geometries, and full 3-D analysis.

2.2.5. Thermo-mechanical analysis

The Thermo-Mechanical characteristics of a TEG device involve the interplay of mechanical stresses and temperature variations. To accurately simulate and analyse these effects, a combination of mechanical and thermal fields must be considered. The following set of equations are central to this analysis:

1. **Stress and Strain Relationship**: The fundamental relationship between stress and strain in a thermo-mechanical system can be expressed through the equation:

$$\overrightarrow{S} = [D]\overrightarrow{\varepsilon} + \overrightarrow{B}\Delta T \tag{11}$$

2. **Strain and Displacement Relationship**: The strain can be related to the displacement field $\overrightarrow{d}$ as follows:

$$\overrightarrow{\varepsilon} = [A]\overrightarrow{d} \tag{12}$$

3. **Energy Equation**: The thermal effects within the material, accounting for both mechanical and thermal fields, can be expressed by:

$$Q = T_k B^T \varepsilon + \rho C_v \Delta T \tag{13}$$

4. **Thermo-Mechanical Coupling**: The coupling between mechanical and thermal fields can be further expressed through:

$$\overrightarrow{B} = [D]\overrightarrow{\beta} \tag{14}$$

2.3. Boundary conditions

Modeling the TEG system necessitates defining accurate boundary conditions that reflect physical constraints and environmental interactions. These conditions ensure the model's real-world relevance, incorporating thermal, electrical, and mechanical interactions. The upcoming sections detail these boundary conditions, pivotal for the TEG's operational analysis.

1. **Hot Side Boundary Condition**:

- **Heat Flux**: A varied heat flux applied to the hot side, representing the different heat sources, depending on the application.

2. **Cold Side Boundary Condition**:

- **Convective Heat Transfer**: The convective heat transfer coefficient is determined based on the nanofluid's thermophysical properties and flow characteristics through the TEG's cold side. The underlying assumptions include laminar fluid flow with minimal influence from different physical properties and the following equations:

The Nusselt number (Nu) is calculated using the Sieder-Tate correlation [57]:

$$Nu = 1.86 \times \left(\frac{\mathrm{Re} \times \mathrm{Pr}}{l/d_e}\right)^{\frac{1}{3}} \tag{15}$$

With the corresponding Reynolds (Re) and Prandtl (Pr) numbers defined as:

$$\mathrm{Pr} = \frac{\rho \nu C_p}{\kappa}; \mathrm{Re} = \frac{u d_e}{\nu} \tag{16}$$

The equivalent diameter and characteristic length are given by:

$$d_e = \frac{4A_f}{B}; l = 0.052\mathrm{m} \tag{17}$$

The heat transfer coefficient (h) is then obtained as:

$$h = \frac{\kappa Nu}{l} \tag{18}$$

Additional assumptions and conditions include:
- Laminar flow of the nanofluid.
- Constant thermophysical properties of the nanofluid.
- Quasi-steady state operation.
- Negligible heat losses due to radiation and conduction.

3. **Electrical Boundary Conditions**:

- **Ground Potential**: The n-type semiconductor is grounded.
- **Floating Potential**: The p-type semiconductor's potential varies dynamically with the Seebeck effect.
- **Terminal Voltage (V)**: Determined by the Seebeck coefficient and current as [41]:

$$V = \alpha \Delta T + IR \tag{19}$$

4. **Thermoelectric Material Properties**:

- **Seebeck Coefficient**, **Electrical Conductivity**, **Thermal Conductivity**: Defined based on temperature-dependent experimental data.

5. **External Load** (R):

- **Load Resistance**: Equal to the internal electrical resistance of the thermoelectric semiconductors.

$$R_{load} = R_{internal} \quad (20)$$

6. **Geometry and Dimensions**:

- Precisely defined for accurate representation, including thickness (1.4 mm), cross-sectional area (1.96 mm^2), and leg length (1.62 mm).

2.4. Model verification

The study's numerical optimization techniques are rigorously verified and validated, ensuring precision and credibility. This approach ensures that optimization insights are grounded in theoretical knowledge and empirical evidence.

2.5. Benchmark comparison

The optimization method is first standardized by comparing our findings with previous theoretical and empirical studies, a benchmarking practice well-established in scholarly literature [58]. This approach validates and strengthens our optimization results. Specifically, our computational methodology replicates outcomes from existing research in concentrating solar thermoelectric technology, with Fig. 3 illustrating this comparative analysis.

2.6. Mesh

2.6.1. Sensitivity analysis

To augment benchmarking, a mesh sensitivity analysis is conducted, confirming the numerical results and determining optimal element sizes for system parameter convergence, like power output. Widely acknowledged in numerical modelling [61], this analysis uses ANSYS's mesh convergence toolbox, crucial for this study. Table 4 presents the results, showing the relationship between grid points and power output at different mesh densities. These comprehensive validation and verification steps collectively reinforce the integrity and robustness of the numerical optimization and the validity of the conclusions drawn.

Table 4
Outcomes of the Mesh Sensitivity Study – Illustration of grid points and corresponding power output (W) at multiple mesh densities.

S/N	Grid Points	Power Output (W)
1	16,437	5.139216
2	30,893	5.139038
3	79,336	5.138978
4	212,573	5.139340
5	513,473	5.139340

3. Results and discussions

This study provides vital insights into the performance of NCSSTEGs with NUCS, especially under dynamic environmental conditions. Employing a comprehensive analysis of various nanofluids and flow velocities, our research offers a deep understanding of the system's exergy, economic, and thermo-mechanical aspects. We explored the impact of both conventional coolants and advanced nanofluids like TiO_2, Fe_3O_4, Al_2O_3, H_2O, and graphene, enhancing our knowledge of effective coolant strategies. The findings determine optimal parameters for concentrated irradiance, skutterudite content, semiconductor dimensions, and load resistance, crucial for improving the system's power and exergy efficiency, economic viability, and overall performance. This research marks a significant step towards sustainable and eco-friendly energy solutions.

3.1. Concentrated irradiance

Fig. 4 presents an analysis of the impact of flow velocities (0.5 m/s to 2 m/s) and different nanofluids on power output under varying solar irradiance levels. Graphene nanofluid at 0.5 m/s achieved the highest power output of 167.59 mW under 550 kWm^{-2} solar irradiance, while TiO_2 showed the lowest at 13.13 mW under 100 kWm^{-2}. Other nanofluids also recorded substantial outputs at elevated irradiance. Power outputs generally increased with higher irradiance, peaking and then slightly decreasing. Graphene's optimal performance was linked to its superior thermal and optical properties, aiding efficient heat removal and enhanced light absorption. Conversely, TiO_2's lower performance is attributed to its lesser thermal conductivity and light absorption efficiency, impacting its power generation potential in the nanofluid-cooled TEG system. The findings regarding the impact of concentrated

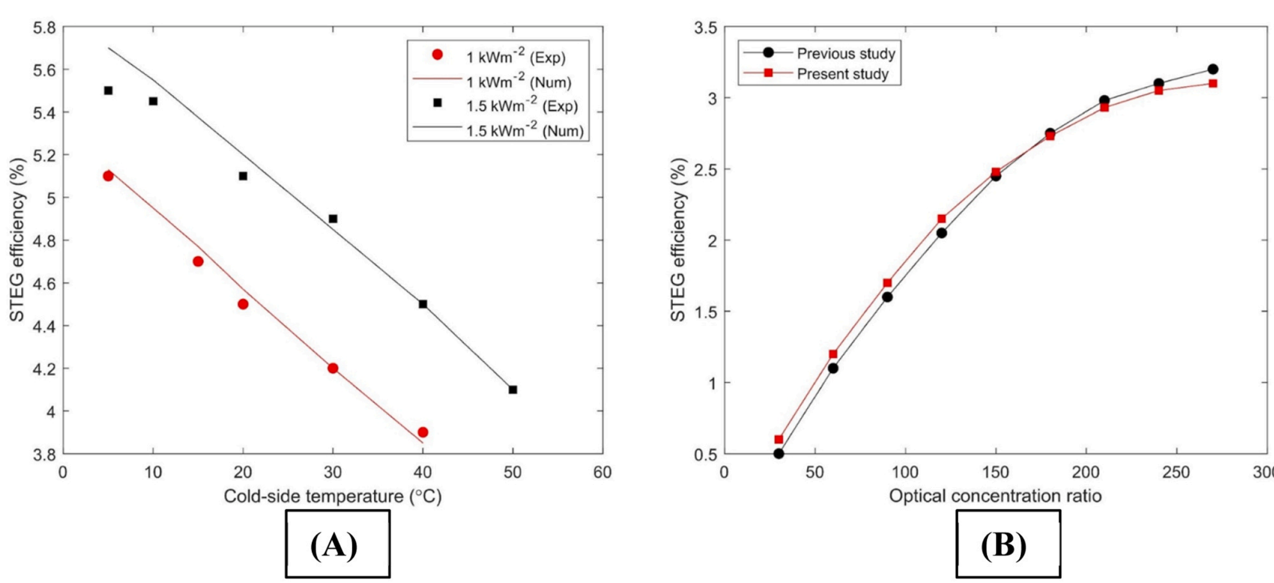

Fig. 3. (A) Side-by-side comparison of the present study's numerical conclusions with empirical data from a previous study involving concentrating solar thermoelectric technology [59]. (B) Correlation of the numerical data with theoretical outcomes from another authoritative research on the same subject [60].

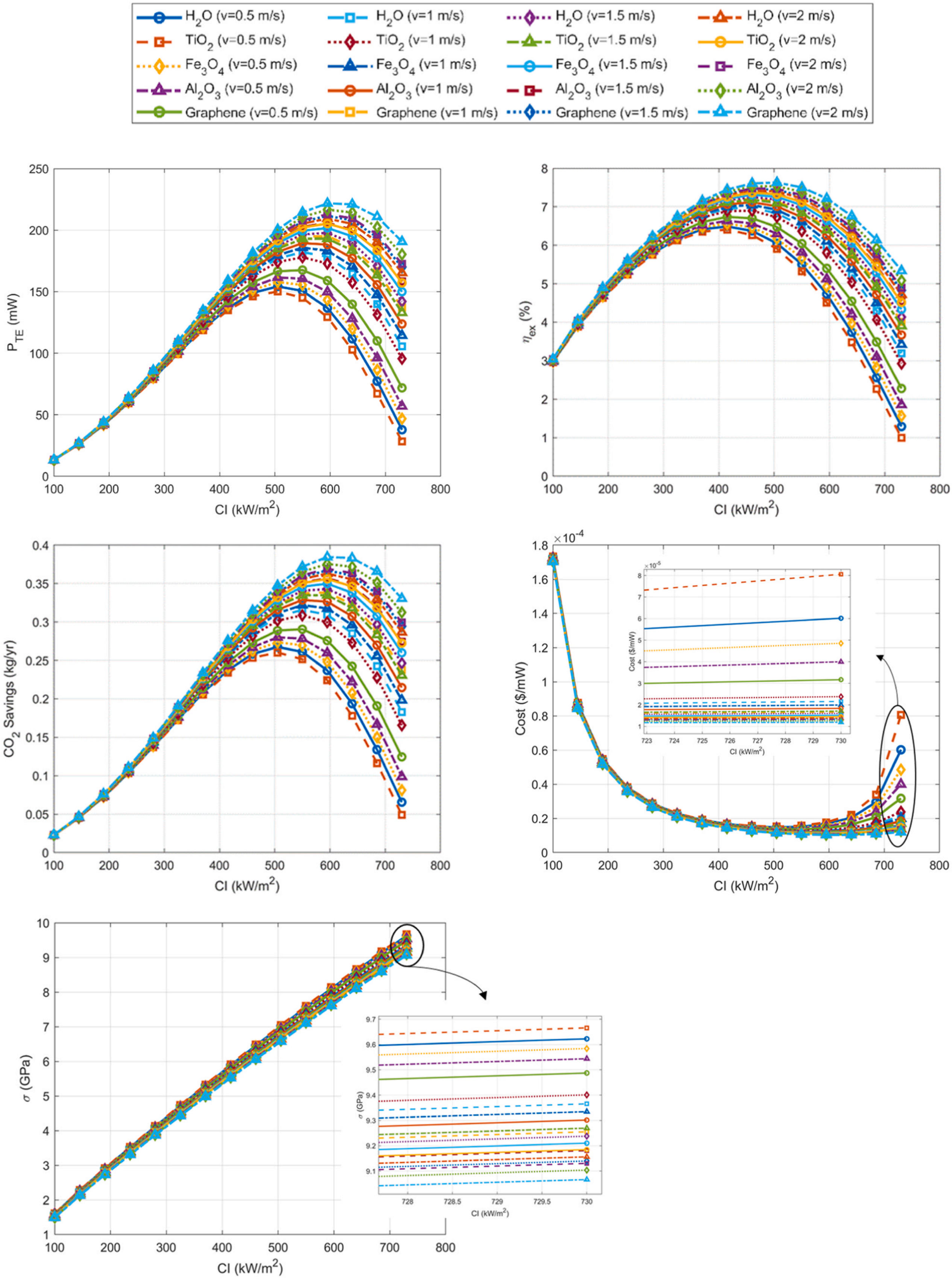

Fig. 4. Combined effects of concentrated irradiance, diverse nanofluids and varying flow velocities on the Power, Exergy Efficiency, CO_2 savings per year, Cost (US dollar) of electrical power, and Maximum von-Mises Stress.

irradiance on power output align with previous studies on solar energy conversion systems. Study by Li et al. [20] similarly observed increased power output with graphene-dispersed nanofluid in TEGs, attributing this trend to enhanced photon absorption and thermal energy transfer.

Furthermore, in a comparative study conducted by Alghamdi et al. [23] on various TEG configurations, it was noted that the PV multi-stage segmented trapezoidal TEG stands out for achieving the highest peak power output using graphene nanofluid cooling at a flow velocity of 2 m/s.

Fig. 4 illustrates the exergy efficiency of NCSSTEGs with NUCS, highlighting the effects of concentrated irradiance, various nanofluids, and flow velocities. Graphene nanofluid demonstrates the highest exergy efficiency, peaking at 7.63 % with a 2 m/s flow velocity under 505 kWm^{-2} irradiances. In contrast, TiO_2 nanofluid shows the lowest efficiency, with a notable decline in performance after peak points. The results emphasize graphene's superior thermal properties and heat dissipation, contributing to its enhanced exergy efficiency. Conversely, TiO_2's limited heat transfer and photon absorption reduce its efficiency. These findings highlight the importance of careful nanofluid selection and optimization in improving solar thermoelectric generators' exergy efficiency and support sustainable solar energy conversion.

This research focuses on optimizing CO_2 savings in NCSSTEGs with NUCS, considering factors like irradiance, nanofluids, and flow velocities (Fig. 4). Graphene nanofluid leads in CO_2 savings, peaking at 0.38 $kgyr^{-1}$ with a 2 m/s flow velocity under 595 kWm^{-2} irradiance, while TiO_2 shows the least savings at various conditions. Graphene's high thermal conductivity and photon absorption enhance thermal energy transfer and power generation, effectively reducing CO_2 emissions. Conversely, TiO_2's limited heat transfer and absorption capabilities result in lower CO_2 savings. These findings emphasize the importance of selecting efficient nanofluids to maximize environmental benefits, guiding the development of sustainable, eco-friendly energy technologies with reduced carbon footprints.

The findings from Fig. 4 demonstrate how concentrated irradiance, diverse nanofluids, and flow velocities affect energy generation cost (in \$/mW) in NCSSTEGs with NUCS. Graphene nanofluid proved most cost-effective at a flow velocity of 0.5 m/s, with the lowest cost of 1.36×10^{-5} \$/mW at 550 kW/m^2 irradiance and 1362.1 W/m^2K^1 heat transfer coefficient. At 1 m/s, graphene-maintained cost-effectiveness at 1.17×10^{-5} \$/mW, while at 1.5 m/s, its cost was 1.08×10^{-5} \$/mW. The most efficient cost at 2 m/s was 1.03×10^{-5} \$/mW, achieved with graphene under 640 kW/m^2 irradiance. Other nanofluids displayed higher costs, around 1.71×10^{-4} \$/mW. These results highlight graphene's superiority in cost-effective energy generation, impacting the economic feasibility and sustainability of the technology. Lower costs with graphene could increase adoption of these generators, supporting renewable energy use and climate change mitigation efforts.

Fig. 4 elucidates how concentrated irradiance, various nanofluids, and flow velocities impact the maximum von-Mises stress in NCSSTEGs. Graphene nanofluid consistently shows lower stress levels, optimizing at 1.49 GPa with a flow velocity of 2 m/s and 100 kWm-2 irradiance. In contrast, TiO_2 nanofluid reaches the highest stress, especially at elevated irradiance levels. The findings suggest that lower irradiance enhances structural integrity, and graphene nanofluid stands out for its mechanical resilience, indicating its suitability for enhancing the system's longevity and stability. The study highlights the significant role of nanofluid type, flow velocity, and irradiance in determining the mechanical stress and stability of these thermoelectric generators.

3.2. Skutterudite content

Fig. 5 illustrates the impact of skutterudite content, nanofluids, and flow velocities on the power generation of NCSSTEGs. Graphene nanofluid consistently outperforms, especially at higher flow velocities, with the highest power output at 2 m/s flow velocity and 37.03 % skutterudite content, achieving 79.39 mW. In contrast, TiO_2 nanofluid shows the lowest power across all scenarios, with its best performance still significantly lower than graphene's. These results indicate that higher skutterudite content and graphene nanofluid use improve power generation, emphasizing the importance of nanofluid selection and flow velocity optimization for efficient solar energy conversion. Findings from studies [62] indicate that the quantity of skutterudite significantly influences the system's power generation capacity and reinforces the significance of skutterudite composition in attaining optimal system performance.

Fig. 5 shows how skutterudite content, nanofluids, and flow velocities affect the exergy efficiency of NCSSTEGs. Exergy efficiency, a measure of energy conversion effectiveness, shows graphene nanofluid achieving the highest efficiency across varying flow velocities, peaking at 8.61 % with 18.51 % skutterudite content at 2 m/s. In contrast, TiO_2 nanofluid consistently exhibits lower exergy efficiency, with the least efficiency at higher skutterudite contents. The study reveals that lower skutterudite content in graphene nanofluid enhances exergy efficiency, indicating the importance of optimizing nanofluid composition. These findings emphasize that selecting appropriate nanofluids and adjusting flow velocities can significantly improve the energy conversion efficiency of these thermoelectric generators.

Fig. 5 examines the influence of skutterudite content, various nanofluids, and flow velocities on CO_2 savings in NCSSTEGs. CO_2 savings, a key environmental metric, showed graphene nanofluid achieving optimal savings at different flow velocities, with the highest at 0.13 $kgyr^{-1}$ for a skutterudite content of 43.20 % at 2 m/s. Increased skutterudite content has been found to have a positive correlation with CO_2 savings, leading to a reduction in the carbon footprint. This observation is consistent with the findings of a recent study [11] where a segmented TEG was optimized to maximize environmental benefits. Conversely, TiO_2 nanofluid showed the least savings across all conditions, highlighting the importance of nanofluid choice for environmental benefits. The study underscores graphene nanofluid's role in enhancing sustainability and reducing CO_2 emissions in solar thermoelectric generators, contributing to eco-friendly energy solutions and climate change mitigation.

Fig. 5 from the research highlights the effects of skutterudite content, different nanofluids, and flow velocities on the cost of electrical power in NCSSTEGs. The study finds that graphene nanofluid, especially at higher skutterudite contents, consistently offers the most cost-effective power generation across various flow velocities. The lowest cost per mW with graphene was observed at 2 m/s flow velocity, showcasing its economic advantage. Conversely, TiO_2 nanofluid exhibited higher costs, especially at lower skutterudite contents. These findings underscore the importance of nanofluid selection and composition in optimizing the economic feasibility of these energy systems, with graphene nanofluid emerging as a favorable option for cost-efficient power generation.

Fig. 5 demonstrates how skutterudite content, nanofluids, and flow velocities affect von-Mises stress in NCSSTEGs. The study finds graphene nanofluid, particularly with higher skutterudite content, consistently minimizes stress, enhancing structural integrity. At a 0.5 m/s flow velocity, graphene nanofluid achieved an optimal stress of 4.15 GPa, suggesting that higher flow velocities and skutterudite contents improve mechanical stability. TiO_2 nanofluid exhibited higher stress levels, especially at lower skutterudite contents and cooling heat transfer coefficients. These findings indicate the importance of nanofluid selection, particularly skutterudite content, in reducing stress and improving the mechanical resilience of thermoelectric generators. Graphene nanofluid stands out for maintaining lower stress across various conditions, offering insights for designing more reliable and efficient thermoelectric systems.

3.3. Semiconductor height

Analyzing Fig. 6, the study investigates the impact of semiconductor height, nanofluids, and flow velocities on power generation in

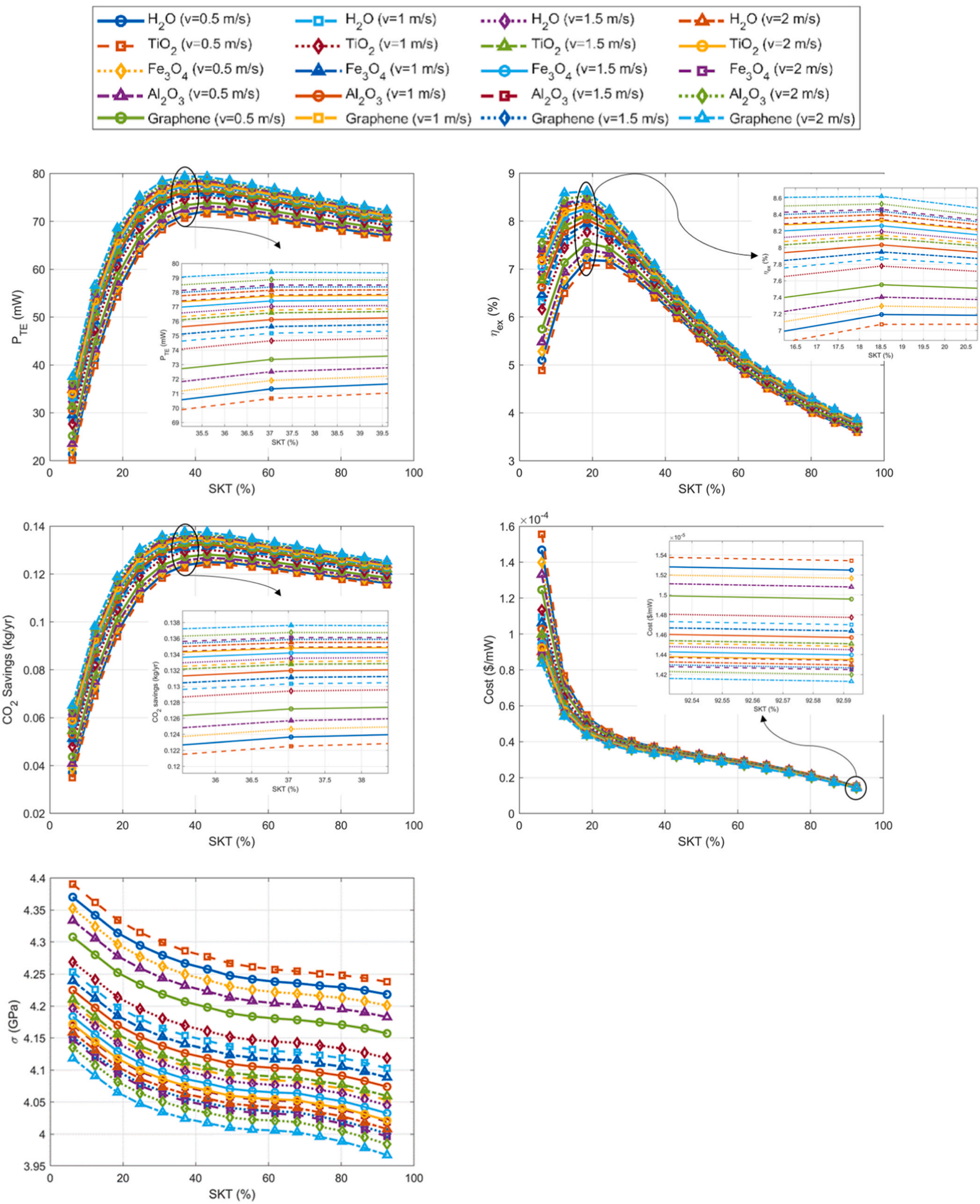

Fig. 5. Combined effects of skutterudite content, diverse nanofluids and varying flow velocities on the Power, Exergy Efficiency, CO_2 savings per year, Cost (US dollar) of electrical power, and Maximum von-Mises Stress.

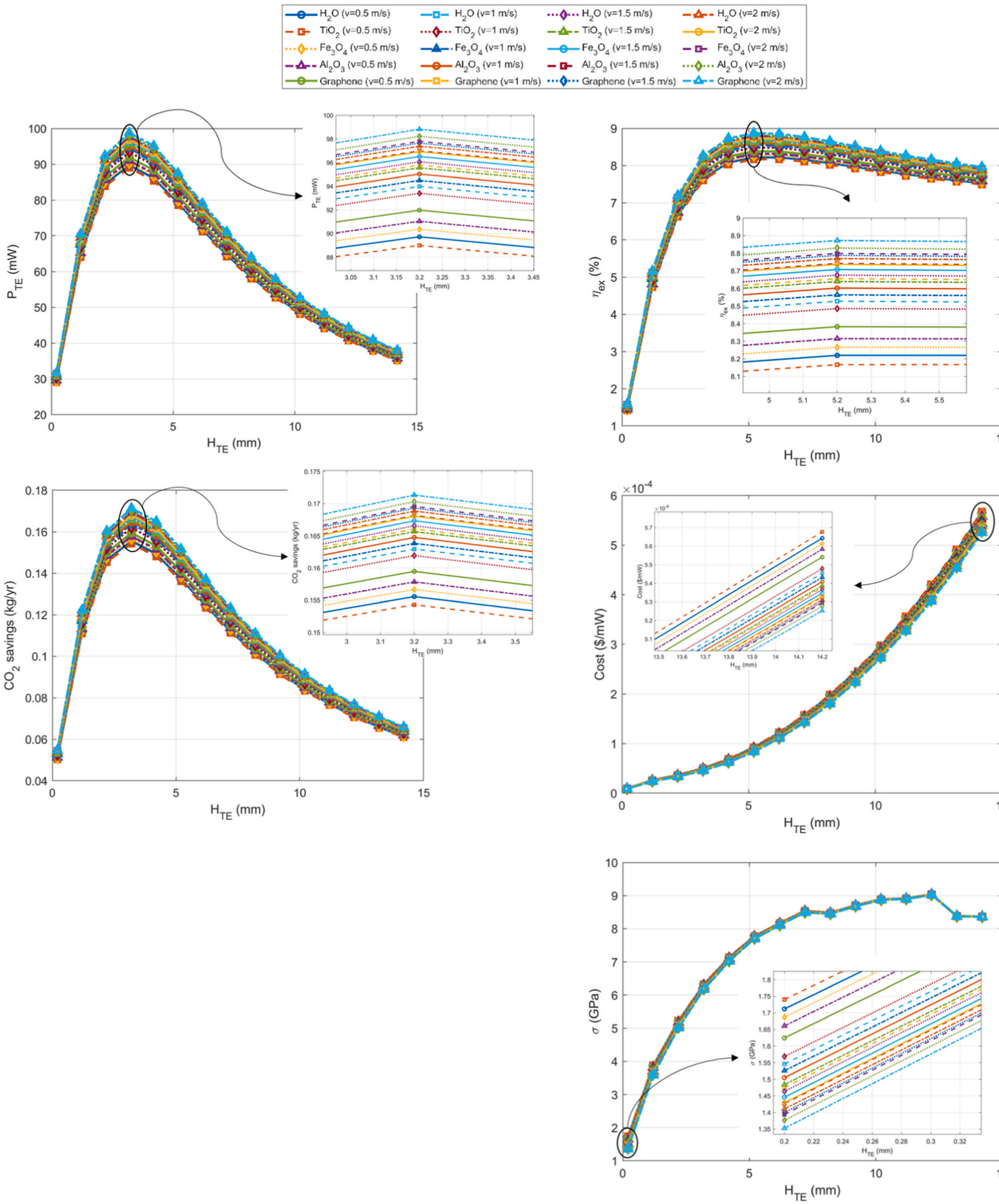

Fig. 6. Combined effects of semiconductor height, diverse nanofluids and varying flow velocities on the Power, Exergy Efficiency, CO_2 savings per year, Cost (US dollar) of electrical power, and Maximum von-Mises Stress.

NCSSTEGs. Higher flow velocities, taller semiconductor heights, and efficient cooling notably enhance power output. Graphene nanofluid consistently outperforms, especially with a semiconductor height of 3.2 mm, achieving optimal power across varying flow velocities. For example, at 0.5 m/s, it generated 91.97 mW, and at 2 m/s, it reached 98.82 mW. In contrast, TiO_2 nanofluid, with a shorter semiconductor height of 0.2 mm, produced significantly less power under similar conditions. The study highlights the crucial roles of semiconductor height and cooling heat transfer coefficient in maximizing power efficiency. These findings underscore the importance of optimizing key parameters like flow velocity, semiconductor height, and cooling efficiency for enhancing the performance of thermoelectric generators.

Fig. 6 delves into how semiconductor height, nanofluids, and flow velocities influence the exergy efficiency of NCSSTEGs. Exergy efficiency, measuring energy conversion effectiveness, improves with higher flow velocities, taller semiconductor heights, and efficient cooling. Graphene nanofluid excels in this aspect, achieving peak exergy efficiency of 8.87 % at a 2 m/s flow velocity, a semiconductor height of 5.2 mm, and a cooling heat transfer coefficient of 2162.1 W/m^2K^1. Conversely, TiO_2 nanofluid shows the lowest efficiency, particularly at shorter semiconductor heights and lower cooling coefficients. These findings underscore the importance of optimizing semiconductor height and cooling mechanisms to maximize exergy efficiency in thermoelectric generators.

Fig. 6 reveals that factors like semiconductor height, nanofluids, and flow velocities significantly impact CO_2 savings in NCSSTEGs, vital for advancing renewable energy and environmental responsibility. Graphene nanofluid, with a semiconductor height of 3.2 mm, consistently demonstrates optimal CO_2 savings across different flow velocities, peaking at 0.17 $kgyr^{-1}$ at 2 m/s. In contrast, TiO_2 nanofluid, especially at a shorter semiconductor height of 0.2 mm, shows the least savings. These results indicate that appropriate selection of nanofluids, semiconductor heights, and flow velocities can significantly enhance CO_2 savings, contributing to eco-friendly energy generation and climate change mitigation. Efficient cooling mechanisms are also crucial, as evidenced by the higher savings achieved with graphene nanofluid at higher cooling coefficients. The findings suggest practical strategies for reducing greenhouse gas emissions, with potential economic benefits in terms of reduced carbon taxes and regulatory compliance costs.

Fig. 6 shows the impact of semiconductor height, nanofluids, and flow velocities on the cost per mW of NCSSTEGs. Graphene nanofluid emerges as the most cost-effective choice, attaining the lowest cost per mW across all flow velocities. For instance, at 0.5 m/s, it achieved an optimal cost of 9.39×10^{-6} $\$mW^{-1}$ at a semiconductor height of 0.2 mm, while TiO_2 nanofluid, with a larger semiconductor height, resulted in a higher cost. This trend continues at higher flow velocities, with graphene consistently maintaining superior economic efficiency. The results highlight the significance of selecting the right nanofluid and semiconductor height for maximizing economic efficiency in these generators. The consistent cost-effectiveness of graphene nanofluid, regardless of flow velocity and semiconductor height, underscores its potential in designing economically viable thermoelectric systems.

Fig. 6 illustrates how semiconductor height, nanofluids, and flow velocities impact the Maximum von-Mises Stress in NCSSTEGs, key to assessing their mechanical performance and structural integrity. Graphene nanofluid consistently shows lower stress values, indicating better mechanical stability. For example, at 0.5 m/s, it achieved an optimal stress of 1.62 GPa at a semiconductor height of 0.2 mm. This trend suggests that lower semiconductor heights contribute to enhanced mechanical resilience. As flow velocity increases, graphene nanofluid maintains favourable stress levels, while higher semiconductor heights in TiO_2 nanofluid lead to increased stresses, potentially affecting structural integrity. The findings emphasize the importance of selecting appropriate nanofluids and semiconductor heights for mechanical stability, with graphene nanofluid offering significant advantages in maintaining lower stress levels, thereby ensuring safer and more reliable operation of the thermoelectric generators.

3.4. Semiconductor cross-section

Fig. 7's findings demonstrate the influence of semiconductor cross-sectional area, nanofluids, and flow velocities on the power output of NCSSTEGs. Graphene nanofluid consistently achieved the highest power output across all flow velocities, especially with smaller semiconductor cross-sectional areas. For example, at 0.5 m/s, it produced an optimal power of 186.34 mW at a cross-sectional area of 0.16 mm^2. In contrast, TiO_2 nanofluid showed lower power outputs with larger cross-sectional areas, highlighting the efficiency of compact semiconductor structures in power generation. The trend persists at higher flow velocities, with graphene nanofluid outperforming others, suggesting its superior heat transfer properties contribute to enhanced power generation. These results indicate the importance of selecting both the appropriate nanofluid and semiconductor dimensions to optimize the energy conversion capabilities of these thermoelectric systems.

Fig. 7's analysis highlights the impact of semiconductor cross-sectional area, nanofluids, and flow velocities on exergy efficiency in NCSSTEGs. Exergy efficiency, measuring energy conversion quality, shows graphene nanofluid outperforming others, particularly with smaller semiconductor cross-sectional areas. For instance, at a flow velocity of 0.5 m/s, graphene achieved an optimal exergy efficiency of 8.54 % with a cross-sectional area of 0.16 mm^2. In contrast, TiO_2 nanofluid exhibited lower efficiency, especially with larger semiconductor cross-sectional areas. This trend continued at higher flow velocities, with graphene nanofluid maintaining superior exergy efficiency, reaching 8.99 % at 2 m/s. These findings suggest that the selection of nanofluids and semiconductor dimensions significantly influences the quality of energy conversion, with graphene nanofluid and compact semiconductor structures enhancing efficiency and minimizing energy waste.

Fig. 7 demonstrates the effectiveness of different nanofluids in enhancing CO_2 savings in NCSSTEGs across various semiconductor cross-sectional areas and flow velocities. Graphene nanofluid stands out as the most effective in reducing CO_2 emissions, highlighting its potential in improving the environmental sustainability of these systems. For example, at a flow velocity of 0.5 m/s and a semiconductor cross-sectional area of 0.16 mm^2, graphene nanofluid achieved the highest CO_2 savings of 0.32 kgyr-1. In contrast, TiO_2 nanofluid, with a larger cross-sectional area of 2.56 mm2, showed the least savings. This trend of graphene nanofluid outperforming others continued at higher flow velocities, with savings ranging from 0.33 to 0.34 $kgyr^{-1}$, while TiO_2 consistently recorded lower savings. These findings underscore the critical role of selecting nanofluids with superior thermal conductivity and heat transfer properties, such as graphene nanofluid, in reducing CO2 emissions and advancing sustainable energy generation.

Fig. 7's analysis of the cost per mW for NCSSTEGs reveals graphene nanofluid as a more economical option compared to TiO2 across various flow velocities and semiconductor cross-sectional areas. For instance, at 0.5 m/s, graphene nanofluid achieved the lowest cost per mW of 3.97×10^{-6} $\$mW^{-1}$ at a cross-sectional area of 0.04 mm^2, while TiO_2 showed higher costs, indicating economic inefficiency. This pattern persists at higher flow velocities, with graphene nanofluid maintaining lower costs, such as 3.79×10^{-6} $\$mW^{-1}$ at 2 m/s. The results underscore the economic benefits of using graphene nanofluid with smaller semiconductor cross-sectional areas, offering cost savings and enhanced sustainability in thermoelectric power generation. Conversely, TiO_2, especially with larger cross-sectional areas, leads to higher power generation costs, highlighting the need to optimize nanofluid properties and system parameters for economic viability.

Fig. 7's analysis on the von-Mises stress, crucial for assessing structural integrity in NCSSTEGs, shows how semiconductor cross-sectional area, nanofluids, and flow velocities interact to affect stress levels. Graphene nanofluid consistently demonstrates optimal stress management across varying flow velocities, particularly with larger semiconductor cross-sectional areas. For instance, at a flow velocity of 0.5 m/s, it achieved an optimal von-Mises stress of 3.99 GPa with a cross-sectional area of 2.56 mm^2. This trend suggests that larger cross-sectional areas can better distribute stress, enhancing material resilience. Conversely, TiO_2 nanofluid exhibited higher stress levels, particularly at smaller cross-sectional areas, underscoring the importance of material selection and system parameter optimization for

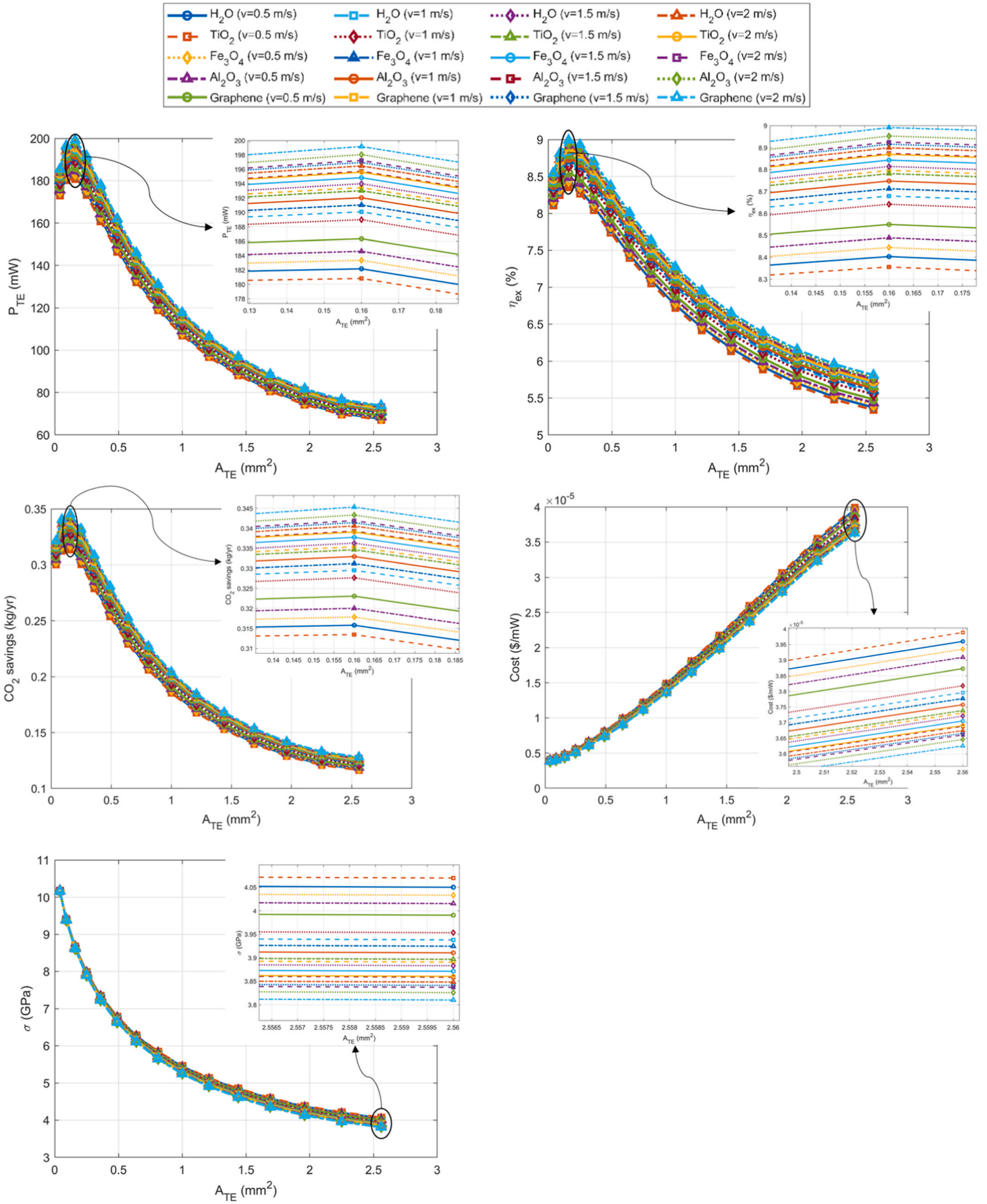

Fig. 7. Combined effects of semiconductor cross-section, diverse nanofluids and varying flow velocities on the Power, Exergy Efficiency, CO_2 savings per year, Cost (US dollar) of electrical power, and Maximum von-Mises Stress.

structural stability. The findings highlight graphene nanofluid's superior performance in maintaining lower stress levels, contributing to the reliability and durability of the thermoelectric generators.

3.5. Load resistance

Fig. 8 shows how load resistance, nanofluids, and flow velocities impact the power output of NCSSTEGs. Graphene nanofluid consistently achieves higher power outputs compared to TiO_2 across various flow velocities and load resistances. For example, at 0.5 m/s, graphene nanofluid reached an optimal power output of 76.42 mW with a load resistance of 0.05 Ω, while TiO_2 only managed 43.50 mW at a lower resistance of 0.01 Ω. As flow velocity increases, the power output with graphene nanofluid continues to improve, hitting 81.48 mW at 2 m/s. This trend indicates that graphene nanofluid is more effective in converting energy at varying flow velocities and load resistances. The study also reveals that power output initially increases with load resistance, then decreases after reaching a peak. This pattern highlights the importance of balancing load resistance with the thermoelectric properties of the materials and flow velocity for optimal energy conversion. The consistent superior performance of graphene nanofluid across the tested conditions underscores its potential in enhancing the efficiency of thermoelectric power generation systems.

Fig. 8 demonstrates how load resistance, nanofluids, and flow velocities influence exergy efficiency in NCSSTEGs. Graphene nanofluid consistently shows superior exergy efficiency across different flow velocities when compared to TiO_2 nanofluid. For instance, at a flow velocity of 0.5 m/s and a load resistance of 0.06 Ω, graphene nanofluid achieved an optimal exergy efficiency of 7.30 %, while TiO2 nanofluid managed only 3.54 % efficiency at a lower resistance of 0.01 Ω. As flow velocity increases, the exergy efficiency with graphene nanofluid continues to improve, reaching 7.72 % at 2 m/s with a load resistance of 0.06 Ω. This trend indicates that graphene nanofluid is more effective in energy conversion at varying flow velocities and load resistances. The

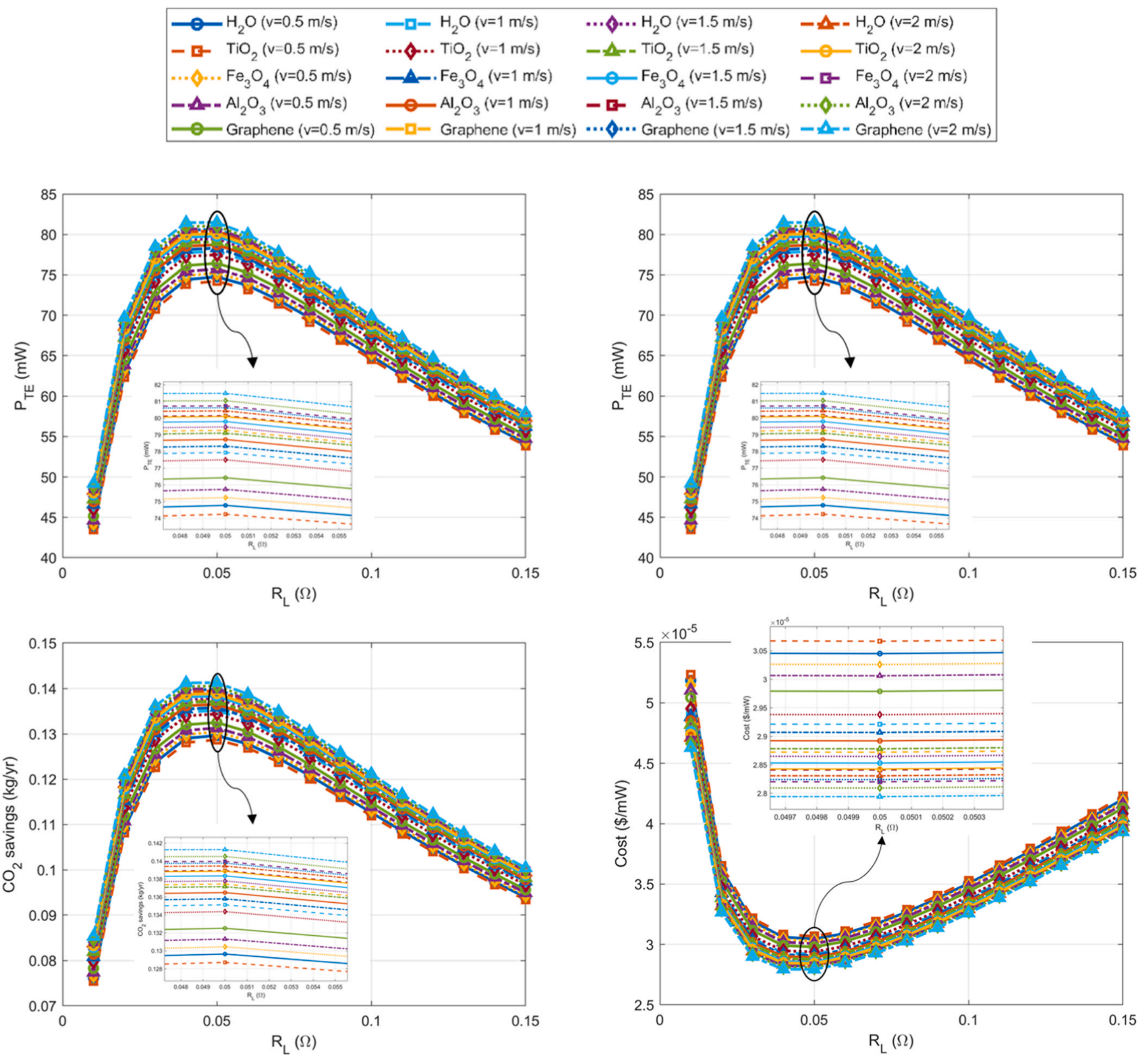

Fig. 8. Combined effects of load resistance, diverse nanofluids and varying flow velocities on the Power, Exergy Efficiency, CO_2 savings per year, & Cost (US dollar) of electrical power.

study also reveals a positive correlation between exergy efficiency and load resistance, suggesting that higher resistance enhances energy conversion quality. These findings highlight the importance of choosing the right combination of nanofluid, load resistance, and flow velocity to optimize exergy efficiency in thermoelectric systems. The consistent superior performance of graphene nanofluid underscores its potential in enhancing the quality and quantity of energy conversion in these systems.

Fig. 8's research on NCSSTEGs shows that load resistance, combined with nanofluid type and flow velocity, significantly impacts CO_2 savings. Graphene nanofluid consistently yielded the highest CO_2 savings across all tested flow velocities, outperforming TiO_2 nanofluid. For instance, at a flow velocity of 0.5 m/s and a load resistance of 0.05 Ω, graphene nanofluid achieved optimal savings of 0.13 $kgyr^{-1}$, whereas TiO_2 nanofluid managed only 0.07 $kgyr^{-1}$. This trend continued at higher flow velocities, with graphene nanofluid maintaining superior CO_2 savings, peaking at 0.14 $kgyr^{-1}$ at 2 m/s. These findings highlight the crucial role of selecting the right nanofluid and adjusting load resistance and flow velocity to optimize CO_2 savings, underlining the importance of sustainable energy conversion for environmental conservation.

Fig. 8's study on NCSSTEGs emphasizes the economic aspect, focusing on "dollars per mW" to evaluate the cost-effectiveness of power generation. Graphene nanofluid consistently demonstrated superior economic efficiency across different flow velocities, outperforming TiO_2 nanofluid. For instance, at 0.5 m/s, graphene achieved an optimal cost of 2.98×10^{-5} \$/mW at a load resistance of 0.05 Ω, while TiO2 was less cost-effective with a higher dollars per mW value. This trend persisted at higher velocities; graphene nanofluid maintained lower costs per mW, culminating in an optimal cost of 2.79×10^{-5} \$/mW at 2 m/s. The study revealed a positive correlation between load resistance and cost efficiency, with an optimum range for load resistance identified for achieving the best economic performance. TiO_2 consistently incurred higher costs for generating power, indicating its lesser viability compared to graphene, especially when considering varying flow velocities and load resistances. These findings highlight the crucial role of selecting suitable nanofluids and optimizing operational parameters to ensure the economic feasibility of thermoelectric power generation systems. Graphene nanofluid, with its lower costs per generated milliwatt under diverse conditions, stands out as an optimal choice for enhancing the cost-effectiveness of these systems.

4. Conclusions

In conclusion, our study represents a significant advancement in the realm of TEG research, particularly focusing on the optimization of segmented NCSSTEGs with nanofluid cooling systems. By meticulously examining various facets of TEG performance and operation, we have contributed valuable insights that have implications for both theoretical understanding and practical applications in sustainable energy systems.

Key Achievements and Contributions:

- Flow Velocity Optimization: The investigation revealed that the implementation of graphene nanofluid cooling at a flow velocity of 2 m/s resulted in exceptional performance enhancements, with the TEG achieving optimal power generation of 221.77 mW and exhibiting a high exergy efficiency of 8.99 %.
- Impact of Concentrated Irradiance: Through rigorous analysis, we demonstrated that graphene nanofluid outperformed other coolant options, particularly at concentrated irradiance levels of 595 kWm^{-2}. This resulted in the highest CO_2 savings of 0.38 $kgyr^{-1}$, depicting the environmental benefits of our proposed cooling approach.
- Efficiency of Semiconductor Cross-Section: Our findings highlighted the economic advantages associated with utilizing graphene nanofluid, as evidenced by its optimal cost-effectiveness ratio of 3.79×10^{-6} \$/mW at a semiconductor cross-section of 0.04 mm^2. This shows the potential for cost savings and enhanced financial viability in TEG applications.
- Thermo-Mechanical Integrity: While the study did not involve direct experimentation, the comprehensive numerical modeling and simulation approach allowed for the thorough evaluation of the structural integrity of the TEG systems under various operating conditions. The findings indicate that graphene nanofluid maintained robustness, exhibiting an optimal von Mises stress of 1.35 GPa at a semiconductor height of 0.2 mm and a flow velocity of 2 m/s. This reinforces the reliability and durability of our proposed cooling strategy.

Overall, this research addresses critical gaps in TEG technology by providing a comprehensive understanding of the interplay between coolant selection, system design, and performance optimization. By bridging theoretical insights with numerical modeling, we have laid the groundwork for future advancements in sustainable energy solutions. Our study not only contributes to the academic discourse but also holds practical implications for the development of efficient and environmentally conscious TEG systems, thereby driving innovation in the field and fostering progress towards a greener future.

5. Future Work

Building on the pivotal discoveries of this study, future research directions for enhancing NCSSTEGs with NUCS include:

1. **Nanofluid Innovation:** Develop advanced nanofluids with superior thermal and thermoelectric properties, exploring diverse nanoparticles and concentrations for optimized TEG system performance.
2. **Environmental Dynamics:** Broaden the model to include dynamic environmental factors like wind, humidity, and solar angles for a more accurate real-world performance assessment.
3. **Thermal Management:** Investigate cutting-edge cooling methods, including phase change materials and microchannel heat exchangers, to boost system efficiency and reliability.
4. **Geometric Optimization:** Conduct in-depth studies to refine the non-uniform cross-section design for enhanced power generation and economic efficiency.
5. **Material Research:** Deepen the study of thermoelectric materials, including novel compounds, to improve thermoelectric efficiency.
6. **Experimental Validation:** Test theoretical models with experimental prototypes under real conditions to confirm practical applicability.
7. **Economic Assessment:** Perform a detailed techno-economic analysis, assessing the system's commercial viability and market potential.
8. **Environmental Analysis:** Extend environmental evaluations to include a full life cycle analysis, providing a comprehensive view of the system's ecological impact and sustainability contribution.

CRediT authorship contribution statement

Chika Maduabuchi: Conceptualization, Writing – original draft, Writing – review & editing.

Declaration of Competing Interest

The authors declare that they have no known competing financial interests or personal relationships that could have appeared to influence the work reported in this paper.

Acknowledgement

The authors extend their appreciation to the Deanship of Scientific Research at Najran University for funding this work under the grant code

NU/NRP/SERC/12/16, the Deanship of Scientific Research at Shaqra University for supporting this work, the Office of Research and Sponsored Programs (ORSP) at Abu Dhabi University for funding this paper through a research fund.

References

[1] Renewable Energy and Jobs – Annual Review 2020", [Online]. Available: https://www.irena.org/- /media/Files/IRENA/Agency/Publication/2020/Sep/IRENA_RE_Jobs_2020.pdf.

[2] L.E. Bell, Cooling, heating, generating power, and recovering waste heat with thermoelectric systems, Science vol. 321 (5895) (Sep. 2008) 1457–1461, https://doi.org/10.1126/science.1158899.

[3] G.J. Snyder, E.S. Toberer, Complex thermoelectric materials. in *Materials for Sustainable Energy*, Co-Published with Macmillan Publishers Ltd, UK, 2010, pp. 101–110, https://doi.org/10.1142/9789814317665_0016.

[4] G.J. Snyder, E.S. Toberer, Complex thermoelectric materials, Nat. Mater. vol. 7 (2) (Feb. 2008) 105–114, https://doi.org/10.1038/nmat2090.

[5] L. Tian, L. Chen, Y. Ge, S. Shi, Maximum efficient power performance analysis and multi-objective optimization of two-stage thermoelectric generators, Entropy vol. 24 (10) (Oct. 2022) 1443, https://doi.org/10.3390/e24101443.

[6] T. Yin, Z.-M. Li, P. Peng, W. Liu, Y.-Y. Shao, Z.-Z. He, Performance analysis of a novel Two-stage automobile thermoelectric generator with the Temperature-dependent materials, Appl. Therm. Eng. vol. 195 (Aug. 2021) 117249, https://doi.org/10.1016/j.applthermaleng.2021.117249.

[7] E. Yousefi, A. Abbas Nejad, M. Khosravi, Experimental investigation of phase change material energy storage system integrated with thermoelectric generator under transient heat loads, Energy Sources Part Recovery Util. Environ. Eff. vol. 44 (3) (Sep. 2022) 6793–6806, https://doi.org/10.1080/15567036.2022.2101717.

[8] F. Li, R. Zhai, Y. Wu, Z. Xu, X. Zhao, T. Zhu, Enhanced thermoelectric performance of n-type bismuth-telluride-based alloys via In alloying and hot deformation for mid-temperature power generation, J. Mater. vol. 4 (3) (Sep. 2018) 208–214, https://doi.org/10.1016/j.jmat.2018.05.008.

[9] R. Wang, Z. Meng, D. Luo, W. Yu, W. Zhou, A comprehensive study on x-type thermoelectric generator modules, J. Electron. Mater. vol. 49 (7) (Jul. 2020) 4343–4354, https://doi.org/10.1007/s11664-020-08152-4.

[10] X. Jia, Y. Gao, Estimation of thermoelectric and mechanical performances of segmented thermoelectric generators under optimal operating conditions, Appl. Therm. Eng. vol. 73 (1) (Dec. 2014) 335–342, https://doi.org/10.1016/j.applthermaleng.2014.07.069.

[11] H. Alghamdi, et al., Pioneering sustainable power: Harnessing material innovations in double stage segmented thermoelectric generators for optimal 4E performance, Appl. Energy vol. 352 (Dec. 2023) 121885, https://doi.org/10.1016/j.apenergy.2023.121885.

[12] H.-B. Liu, J.-H. Meng, X.-D. Wang, W.-H. Chen, A new design of solar thermoelectric generator with combination of segmented materials and asymmetrical legs, Energy Convers. Manag. vol. 175 (Nov. 2018) 11–20, https://doi.org/10.1016/j.enconman.2018.08.095.

[13] Y.-Q. Zhang, J. Sun, G.-X. Wang, T.-H. Wang, Advantage of a thermoelectric generator with hybridization of segmented materials and irregularly variable cross-section design, Energies vol. 15 (8) (Apr. 2022) 2944, https://doi.org/10.3390/en15082944.

[14] Y. Luo, L. Li, Y. Chen, C.N. Kim, Influence of geometric parameter and contact resistances on the thermal-electric behavior of a segmented TEG, Energy vol. 254 (Sep. 2022) 124487, https://doi.org/10.1016/j.energy.2022.124487.

[15] S. Shittu, G. Li, X. Zhao, X. Ma, Y.G. Akhlaghi, E. Ayodele, Optimized high performance thermoelectric generator with combined segmented and asymmetrical legs under pulsed heat input power, J. Power Sources vol. 428 (Jul. 2019) 53–66, https://doi.org/10.1016/j.jpowsour.2019.04.099.

[16] C.A. Mgbemene, J. Duffy, H. Sun, S.O. Onyegegbu, Electricity Generation From a Compound Parabolic Concentrator Coupled to a Thermoelectric Module. in *ASME 2008 2nd International Conference on Energy Sustainability, Volume 2*, Jacksonville, Florida, USA: ASMEDC, Jan. 2008, pp. 423–432, https://doi.org/10.1115/ES2008-54122.

[17] S. Wiriyasart, P. Suksusron, C. Hommalee, A. Siricharoenpanich, P. Naphon, Heat transfer enhancement of thermoelectric cooling module with nanofluid and ferrofluid as base fluids, Case Stud. Therm. Eng. vol. 24 (Apr. 2021) 100877, https://doi.org/10.1016/j.csite.2021.100877.

[18] Z. Li, W. Li, Z. Chen, Performance analysis of thermoelectric based automotive waste heat recovery system with nanofluid coolant, Energies vol. 10 (10) (Sep. 2017) 1489, https://doi.org/10.3390/en10101489.

[19] M.N.H.M. Hilmin, M.F. Remeli, B. Singh, N.D.N. Affandi, Thermoelectric power generations from vehicle exhaust gas with TiO2 nanofluid cooling, Therm. Sci. Eng. Prog. vol. 18 (Aug. 2020) 100558, https://doi.org/10.1016/j.tsep.2020.100558.

[20] J. Xing, Z. Wu, H. Xie, Y. Wang, Y. Li, J. Mao, Performance of thermoelectric generator with graphene nanofluid cooling, Chin. Phys. B vol. 26 (10) (Sep. 2017) 104401, https://doi.org/10.1088/1674-1056/26/10/104401.

[21] H. Alghamdi, et al., Latest advancements in solar photovoltaic-thermoelectric conversion technologies: thermal energy storage using phase change materials, machine learning, and 4E analyses, Int. J. Energy Res. vol. 2024 (Jan. 2024) 1–29, https://doi.org/10.1155/2024/1050785.

[22] S. Aberoumand, S. Ghamari, B. Shabani, Energy and exergy analysis of a photovoltaic thermal (PV/T) system using nanofluids: An experimental study, Sol. Energy vol. 165 (May 2018) 167–177, https://doi.org/10.1016/j.solener.2018.03.028.

[23] H. Alghamdi, et al., Performance optimization of nanofluid-cooled photovoltaic-thermoelectric systems: a study on geometry configuration, steady-state and annual transient effects, Energy vol. 296 (Jun. 2024) 131022, https://doi.org/10.1016/j.energy.2024.131022.

[24] H. Ruan, et al., Numerical investigation and comparative analysis of nanofluid cooling enhancement for TEG and TEC systems, Case Stud. Therm. Eng. vol. 27 (Oct. 2021) 101331, https://doi.org/10.1016/j.csite.2021.101331.

[25] C.A. Mgbemene, H.O. Njoku, C.O.A. Agbo, Investigation of Parametric Performance of the Hybrid 3D CPC/TEM System Due to Thermoelectric Irreversibilities, Front. Energy Res. vol. 6 (Oct. 2018) 101, https://doi.org/10.3389/fenrg.2018.00101.

[26] U. Erturun, K. Erermis, K. Mossi, Effect of various leg geometries on thermo-mechanical and power generation performance of thermoelectric devices, Appl. Therm. Eng. vol. 73 (1) (Dec. 2014) 128–141, https://doi.org/10.1016/j.applthermaleng.2014.07.027.

[27] U. Erturun, K. Erermis, K. Mossi, Influence of leg sizing and spacing on power generation and thermal stresses of thermoelectric devices, Appl. Energy vol. 159 (Dec. 2015) 19–27, https://doi.org/10.1016/j.apenergy.2015.08.112.

[28] C.C. Maduabuchi, C.A. Mgbemene, Numerical study of a phase change material integrated solar thermoelectric generator, J. Electron. Mater. vol. 49 (10) (Oct. 2020) 5917–5936, https://doi.org/10.1007/s11664-020-08331-3.

[29] G. Li, et al., Brittle failure mechanism in thermoelectric skutterudite $CoSb_3$, Chem. Mater. vol. 27 (18) (Sep. 2015) 6329–6336, https://doi.org/10.1021/acs.chemmater.5b02268.

[30] L. Chen, J. Lee, Effect of pulsed heat power on the thermal and electrical performances of a thermoelectric generator, Appl. Energy vol. 150 (Jul. 2015) 138–149, https://doi.org/10.1016/j.apenergy.2015.04.009.

[31] S. Fan, Y. Gao, Numerical analysis on the segmented annular thermoelectric generator for waste heat recovery, Energy vol. 183 (Sep. 2019) 35–47, https://doi.org/10.1016/j.energy.2019.06.103.

[32] T. Caillat, A. Borshchevsky, J.-P. Fleurial, Properties of single crystalline semiconducting CoSb3, J. Appl. Phys. vol. 80 (8) (Oct. 1996) 4442–4449, https://doi.org/10.1063/1.363405.

[33] J.-L. Gao, Q.-G. Du, X.-D. Zhang, X.-Q. Jiang, Thermal stress analysis and structure parameter selection for a Bi2Te3-based thermoelectric module, J. Electron. Mater. vol. 40 (5) (May 2011) 884–888, https://doi.org/10.1007/s11664-011-1611-3.

[34] X. Yang, P. Zhai, L. Liu, Q. Zhang, Thermodynamic and mechanical properties of crystalline CoSb3: a molecular dynamics simulation study, J. Appl. Phys. vol. 109 (12) (Jun. 2011) 123517, https://doi.org/10.1063/1.3598116.

[35] A.S. Al-Merbati, B.S. Yilbas, A.Z. Sahin, Thermodynamics and thermal stress analysis of thermoelectric power generator: influence of pin geometry on device performance, Appl. Therm. Eng. vol. 50 (1) (Jan. 2013) 683–692, https://doi.org/10.1016/j.applthermaleng.2012.07.021.

[36] L. Syam Sundar, M.K. Singh, A.C.M. Sousa, Investigation of thermal conductivity and viscosity of Fe3O4 nanofluid for heat transfer applications, Int. Commun. Heat. Mass Transf. vol. 44 (May 2013) 7–14, https://doi.org/10.1016/j.icheatmasstransfer.2013.02.014.

[37] M.A. Abdelkareem, et al., Prospects of thermoelectric generators with nanofluid, Therm. Sci. Eng. Prog. vol. 29 (Mar. 2022) 101207, https://doi.org/10.1016/j.tsep.2022.101207.

[38] N. Ahammed, L.G. Asirvatham, S. Wongwises, Thermoelectric cooling of electronic devices with nanofluid in a multiport minichannel heat exchanger, Exp. Therm. Fluid Sci. vol. 74 (Jun. 2016) 81–90, https://doi.org/10.1016/j.expthermflusci.2015.11.023.

[39] C. Maduabuchi, Improving the performance of a solar thermoelectric generator using nano-enhanced variable area pins, Appl. Therm. Eng. vol. 206 (Apr. 2022) 118086, https://doi.org/10.1016/j.applthermaleng.2022.118086.

[40] C. Maduabuchi, Thermo-mechanical optimization of thermoelectric generators using deep learning artificial intelligence algorithms fed with verified finite element simulation data, Appl. Energy vol. 315 (Jun. 2022) 118943, https://doi.org/10.1016/j.apenergy.2022.118943.

[41] C. Maduabuchi, et al., Thomson effect and nonlinear performance of thermoelectric generator, Heat. Mass Transf. vol. 58 (6) (Jun. 2022) 967–980, https://doi.org/10.1007/s00231-021-03153-3.

[42] C. Badillo-Ruiz, M. Olivares-Robles, P. Ruiz-Ortega, Performance of segmented thermoelectric cooler micro-elements with different geometric shapes and temperature-dependent properties, Entropy vol. 20 (2) (Feb. 2018) 118, https://doi.org/10.3390/e20020118.

[43] S. Singh, O.I. Ibeagwu, R. Lamba, Thermodynamic evaluation of irreversibility and optimum performance of a concentrated PV-TEG cogenerated hybrid system, Sol. Energy vol. 170 (Aug. 2018) 896–905, https://doi.org/10.1016/j.solener.2018.06.034.

[44] G. Fraisse, J. Ramousse, D. Sgorlon, C. Goupil, Comparison of different modeling approaches for thermoelectric elements, Energy Convers. Manag. vol. 65 (Jan. 2013) 351–356, https://doi.org/10.1016/j.enconman.2012.08.022.

[45] C.C. Maduabuchi, K.A. Ejenakevwe, C.A. Mgbemene, Performance optimization and thermodynamic analysis of irreversibility in a contemporary solar thermoelectric generator, Renew. Energy vol. 168 (May 2021) 1189–1206, https://doi.org/10.1016/j.renene.2020.12.130.

[46] S.C. Kaushik, S. Manikandan, R. Hans, Energy and exergy analysis of an annular thermoelectric heat pump, J. Electron. Mater. vol. 45 (7) (Jul. 2016) 3400–3409, https://doi.org/10.1007/s11664-016-4465-x.

[47] C.C. Maduabuchi, R. Lamba, M. Eke, E. Ejiogu, Multi-dimensional optimization of a concentrated solar thermoelectric generator, Int. J. Energy Res. vol. 46 (5) (Apr. 2022) 5896–5907, https://doi.org/10.1002/er.7530.
[48] M.N. Eke, et al., Exergy analysis and optimisation of a two-stage solar thermoelectric generator with tapered legs, Int. J. Exergy vol. 38 (1) (2022) 110, https://doi.org/10.1504/IJEX.2022.122309.
[49] R. Petela, Exergy of undiluted thermal radiation, Sol. Energy vol. 74 (6) (Jun. 2003) 469–488, https://doi.org/10.1016/S0038-092X(03)00226-3.
[50] C. Maduabuchi, H. Njoku, M. Eke, C. Mgbemene, R. Lamba, J.S. Ibrahim, Overall performance optimisation of tapered leg geometry based solar thermoelectric generators under isoflux conditions, J. Power Sources vol. 500 (Jul. 2021) 229989, https://doi.org/10.1016/j.jpowsour.2021.229989.
[51] H. Alghamdi, et al., Machine learning model for transient exergy performance of a phase change material integrated-concentrated solar thermoelectric generator, Appl. Therm. Eng. vol. 228 (Jun. 2023) 120540, https://doi.org/10.1016/j.applthermaleng.2023.120540.
[52] H. Alghamdi, et al., Multiobjective optimization and machine learning algorithms for forecasting the 3E performance of a concentrated photovoltaic-thermoelectric system, Int. J. Energy Res. vol. 2023 (Mar. 2023) 1–22, https://doi.org/10.1155/2023/6418897.
[53] Emissions – Global Energy & CO2 Status Report 2019 – Analysis - IEA." Accessed: Sep. 24, 2023. [Online]. Available: ⟨https://www.iea.org/reports/global-energy-co2-status-report-2019/emissions⟩.
[54] S.K. Yee, S. LeBlanc, K.E. Goodson, C. Dames, $ per W metrics for thermoelectric power generation: beyond ZT, Energy Env. Sci. vol. 6 (9) (Jun. 2013) 2561–2571, https://doi.org/10.1039/C3EE41504J.
[55] E.E. Antonova, D.C. Looman, Finite elements for thermoelectric device analysis in ANSYS. in *ICT 2005. 24th International Conference on Thermoelectrics, 2005.*, Clemson, SC, USA: IEEE, 2005, pp. 215–218, https://doi.org/10.1109/ICT.2005.1519922.
[56] G.J. Snyder, J.-P. Fleurial, T. Caillat, R. Yang, G. Chen, Supercooling of Peltier cooler using a current pulse, J. Appl. Phys. vol. 92 (3) (Aug. 2002) 1564–1569, https://doi.org/10.1063/1.1489713.
[57] E.N. Sieder, G.E. Tate, Heat Transfer and Pressure Drop of Liquids in Tubes, Ind. Eng. Chem. vol. 28 (12) (Dec. 1936) 1429–1435, https://doi.org/10.1021/ie50324a027.
[58] Y. Cai, B.-H. Hong, S.-Q. Zhuang, R.-B. An, W.-X. Wu, F.-Y. Zhao, Numerical analysis of a solar driven thermoelectric generator brick with phase change materials: Performance evaluation and parametric investigations, Appl. Therm. Eng. vol. 214 (Sep. 2022) 118879, https://doi.org/10.1016/j.applthermaleng.2022.118879.
[59] D. Kraemer, et al., High-performance flat-panel solar thermoelectric generators with high thermal concentration, Nat. Mater. vol. 10 (7) (Jul. 2011) 532–538, https://doi.org/10.1038/nmat3013.
[60] D.N. Kossyvakis, C.G. Vossou, C.G. Provatidis, E.V. Hristoforou, Computational analysis and performance optimization of a solar thermoelectric generator, Renew. Energy vol. 81 (Sep. 2015) 150–161, https://doi.org/10.1016/j.renene.2015.03.026.
[61] A. Johansson, B. Kehlet, M.G. Larson, A. Logg, Multimesh finite element methods: Solving PDEs on multiple intersecting meshes, Comput. Methods Appl. Mech. Eng. vol. 343 (Jan. 2019) 672–689, https://doi.org/10.1016/j.cma.2018.09.009.
[62] H. Alghamdi, et al., Beyond traditional boundaries: exergo-economic and thermo-mechanical optimization of segmented thermoelectric generators with varied cross-sections, J. Power Sources vol. 581 (Oct. 2023) 233500, https://doi.org/10.1016/j.jpowsour.2023.233500.